

This document is confidential and is proprietary to the American Chemical Society and its authors. Do not copy or disclose without written permission. If you have received this item in error, notify the sender and delete all copies.

Synergy of Two Assembly Languages in DNA Nanostructures: Self-Assembly of Sequence-Defined Polymers on DNA Cages

Journal:	<i>Journal of the American Chemical Society</i>
Manuscript ID	ja-2015-12953d.R1
Manuscript Type:	Article
Date Submitted by the Author:	08-Mar-2016
Complete List of Authors:	Chidchob, Pongphak; McGill University, Chemistry Edwardson, Thomas; McGill University, Chemistry Serpell, Christopher; McGill University, Department of Chemistry Sleiman, Hanadi; McGill University, Department of Chemistry

SCHOLARONE™
Manuscripts

Synergy of Two Assembly Languages in DNA Nanostructures: Self-Assembly of Sequence-Defined Polymers on DNA Cages

Pongphak Chidchob, Thomas G. W. Edwardson, Christopher J. Serpell, & Hanadi F. Sleiman*

Department of Chemistry and Centre for Self-Assembled Chemical Structures (CSACS-CRMAA), McGill University, 801 Sherbrooke Street West, Montreal, Quebec H3A 0B8, Canada

Abstract

DNA base-pairing is the central interaction in DNA assembly. However, this simple four-letter (A-T and G-C) language makes it difficult to create complex structures without using a large number of DNA strands of different sequences. Inspired by protein folding, we introduce hydrophobic interactions to expand the assembly language of DNA nanotechnology. To achieve this, DNA cages of different geometries are combined with sequence-defined polymers containing long alkyl and oligoethylene glycol repeat units. Anisotropic decoration of hydrophobic polymers on one face of the cage leads to hydrophobically-driven formation of quantized aggregates of DNA cages, where polymer length determines the cage aggregation number. Hydrophobic chains decorated on both faces of the cage can undergo an intra-scaffold 'handshake' to generate DNA-micelle cages, which have increased structural stability and assembly cooperativity, and can encapsulate small molecules. The polymer sequence order can control the interaction between hydrophobic blocks, leading to unprecedented 'doughnut-shaped' DNA cage-ring structures. We thus demonstrate that new structural and functional modes in DNA nanostructures can emerge from the synergy of two interactions, providing an attractive approach to develop protein-inspired assembly modules in DNA nanotechnology.

Introduction

Sequence-controlled polymers, such as oligonucleotides and polypeptides, are remarkable macromolecules in which the order of the building blocks along the polymer chain provides all necessary instructions for efficient structural control, molecular recognition and catalysis.¹ In particular, polypeptide chains are programmed to fold themselves into final predetermined structures with very high accuracy to construct important **biological** nanomachines. Although such a level of structural and functional complexity has not been fully realized synthetically,¹ the field of DNA nanotechnology offers a powerful tool to create finely designed two- and three-dimensional architectures and devices by using DNA as the main building block.²⁻¹¹ However, a large number of DNA strands of unique sequences are generally required for the assembly of more complex structures. This decreases scalability and can **theoretically** increase assembly errors, due to the limited four-letter A-T and G-C ‘language’ in DNA assembly.

The incorporation of multiple molecular interactions within the same building block is an efficient strategy to achieve complex and hierarchical assembly in biological systems. Of these, hydrophobic interactions are the underlying mechanism for many structural elements in biology such as phospholipid bilayers, vesicles and many proteins. They are also a fundamental driving force for the self-assembly of synthetic block copolymers into various morphologies such as spherical micelles, cylindrical micelles and vesicles.¹² The integration of hydrophobic interactions with DNA base-pairing is a promising approach not only to overcome the complexity-scalability-error issues, but also to introduce new assembly modes and functionalities in DNA assembly.^{13,14} Inspired by protein folding, we would like to create assembly modules, like protein coiled-coil motifs, as elementary repeats in DNA nanotechnology, thus we need to understand the rules governing the interplay between the two languages in the assembly. However, one of the problems is the difficulty in the synthesis of DNA conjugated with hydrophobic molecules and polymers. Our group has recently developed an automated solid-phase synthesis to prepare monodisperse DNA-polymer conjugates based on phosphoramidite chemistry.¹⁵ This approach is not only convenient, rapid and high yielding but also allows one to place functional monomers in a sequence-controlled manner on the polymer backbone.

The combination of DNA base-pairing with hydrophobic interactions can expand assembly modes to DNA nanostructures which would not be possible otherwise. DNA cages have emerged as promising platform for cellular delivery of therapeutics.¹⁶⁻²⁰ However, unmodified DNA/RNA structures suffer from nuclease instability, poor cellular penetration and rapid clearance *in vivo*.¹⁶⁻²⁰ Attaching hydrophobic functionalities and increasing the assembly range of DNA cages can be an effective method to overcome these barriers. To our knowledge, the implementation of hydrophobic interactions in the

1
2
3 design of DNA nanostructures is still considerably unexplored. Some examples that integrate
4 hydrophobic interactions with DNA nanostructures include self-folding of DNA rectangles mediated by
5 cholesterol²¹ and hydrophobic dendritic molecules,²² and DNA tetrahedra functionalized with a
6 thermoresponsive polymer that can transition between a discrete tetrahedron and giant-surfactant
7 aggregates.²³ Recent work by our group has demonstrated the significant role of hydrophobic interactions
8 in directing the association of alkyl chains on three-dimensional DNA scaffolds. The number and position
9 of the chains on DNA cubes can dramatically alter their assembly behavior.^{14,24}

10
11
12
13
14
15
16 In this article, we report an in-depth study of the self-assembly of sequence-defined hydrophobic
17 polymers on DNA cages (Figure 1). Our system allows the systematic change of cage structure and size,
18 and orientation of individual polymer chains on the DNA scaffold. On the polymer end, the polymers are
19 monodisperse and sequence controlled in such a way that we can precisely change the number of
20 hydrophobic repeats, the relative number of hydrophilic to hydrophobic repeats, and the polymer
21 sequence. We found that decoration of the polymers on the cages leads to new DNA super-structures
22 through hierarchical assembly, via DNA base-pairing and hydrophobic interactions. (i) Short hydrophobic
23 chains result in *monomeric DNA cage structures*. (ii) Intermediate chains arranged on one face of the
24 DNA cage result in *quantized cage assemblies*, where a specific number of DNA cages is organized
25 around a hydrophobic core; here, the number of repeats in the polymer defines the size of the hydrophobic
26 core, and dictates number of DNA cages that form these aggregates. (iii) Hydrophobic chains on both
27 faces of the cage undergo an intra-scaffold ‘handshake’, to give *DNA-micelle cages*. Hydrophobic
28 interactions not only mediate the encapsulation of small molecules in the cage, but also significantly
29 increase structural stability and assembly cooperativity. (iv) Specific polymer sequences result in
30 unprecedented *doughnut-shaped DNA cage-ring structures*, where DNA cages are organized into rings,
31 whose diameter and density can be controlled by varying the length of the polymer blocks. We propose a
32 mechanism for the hydrophobically-driven quantized self-assembly that is dependent on the chain length
33 of the polymers, and we study the dynamic ability of the quantized DNA cage assemblies to undergo
34 structural exchange. We thus demonstrate the efficient use of sequence-defined hydrophobic polymers to
35 create orthogonal assembly modes which synergistically combine hydrophobic and base pairing
36 interactions in the assembly of DNA nanostructures.
37
38
39
40
41
42
43
44
45
46
47
48
49
50
51
52
53
54
55
56
57
58
59
60

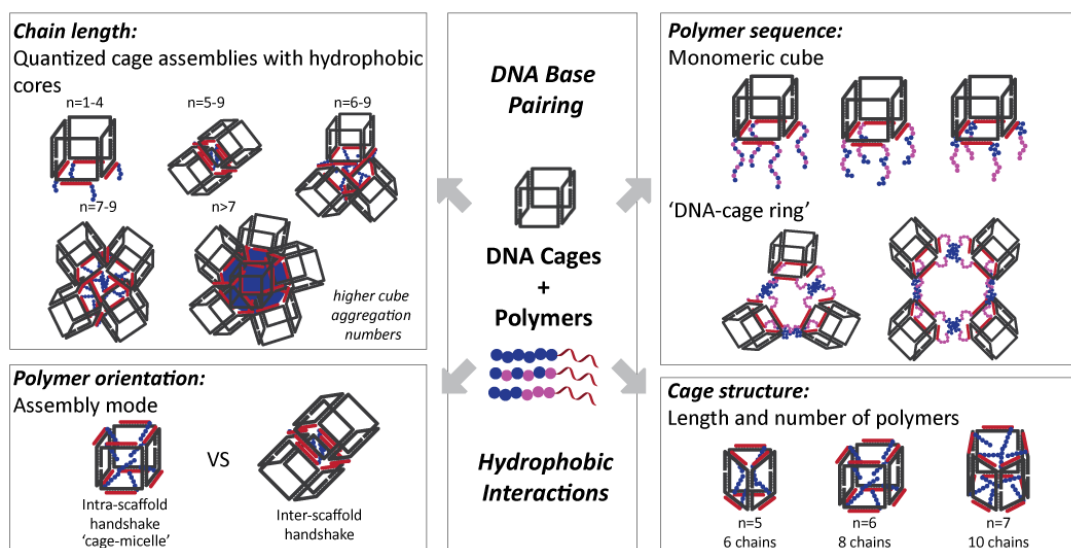


Figure 1. Schematic representation of the self-assembly of sequence-defined hydrophobic polymers on DNA cages. The blue and magenta circles denote hydrophobic and hydrophilic monomers along the polymer chains, where 'n' is the number of hydrophobic repeats. *Top Left*, Hydrophobic polymers on one face of DNA cage lead to 'quantized cage assemblies', whose aggregation number depends on the number of hydrophobic polymer repeats. *Top right*, Depending on their sequence, polymers with hydrophilic and hydrophobic repeats give monomeric cages, or donut-shaped 'cage-rings'. *Bottom left*, when both faces of the DNA cage have hydrophobic polymers, they can undergo an intra-scaffold 'handshake' into a 'cage-micelle' that encapsulates small molecules and is significantly more stable than the unsubstituted cage. *Bottom right*, depending on cage geometry, the intra-scaffold 'handshake' occurs with a different number of hydrophobic polymer repeats, with different capacity for small molecules.

Results and discussion

Design of DNA cages and sequence-defined DNA-polymer conjugates

DNA cages were chosen as scaffolds for three-dimensional positioning of DNA-polymer conjugates and were assembled *via* a 'clip-by-clip' approach.^{14,24} The clips are 80-mer DNA strands composed of four single-stranded segments separated by a hexaethyloxy-glycol (HEG) spacer. The 20-mer segment in the middle of the clip can hybridize to two peripheral 10-mer segments of the next clip. Cube (C) can be constructed from four clips where the fourth clip folds back and hybridizes to the first clip, cyclizing the cubic assembly (Figure 2a). This structure presents 8 20-mer segments that are single-stranded, and provide binding sites for DNA-polymer conjugates. In a similar approach, triangular prism

(TP) and pentagonal prism (PP) can be generated from three and five clips, respectively, and structures were generated in quantitative or near quantitative yields (see Section V in Supporting Information).

To prepare sequence-defined DNA-polymer conjugates, 1,12-dodecane-diol (hexaethylene, HE) and hexaethyloxy-glycol (HEG) were chosen as hydrophobic and hydrophilic monomers (Figure 2b). These monomers were attached to a 19-mer DNA by automated solid-phase synthesis using phosphoramidite chemistry.¹⁵ The DNA segments contain a 5T spacer and 14-mer complementary sequence to the single-stranded segments on the cages. A series of DNA-HE conjugates and DNA-HE/HEG copolymer conjugates were synthesized to systematically investigate the design parameters of DNA-polymer conjugates for their assembly behavior on DNA cages (Figure 1b, and see Section IV in Supporting Information).

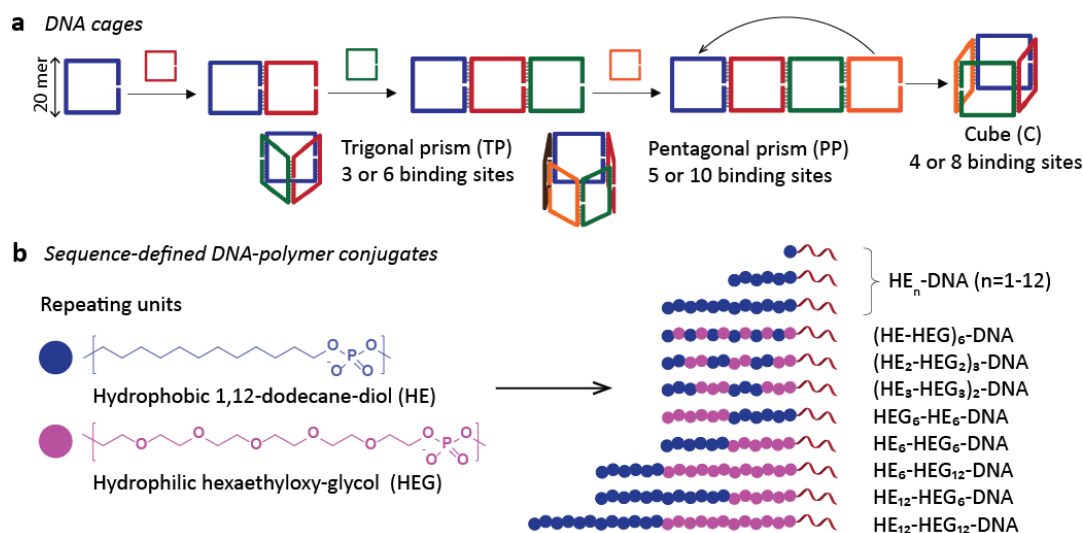


Figure 2. Cage and DNA-polymer conjugate design. a) Clip-by-clip approach for DNA cage construction. A cube can be constructed from four different 80-mer DNA clips and contains maximum of 8 binding sites. b) Hydrophilic hexaethyloxy-glycol (HEG) and hydrophobic 1,12-dodecane-diol (HE) monomers for the synthesis of sequence-defined DNA-polymer conjugates. The 14-mer single-stranded DNA can hybridize to the single-stranded segments on the cages.

Polymers: number of hydrophobic repeats

We had previously decorated DNA cubes with dendritic alkyl chains, and showed that a cube with 4 dendritic units on one of its faces can associate into a dimer via an intermolecular ‘handshake’ of the hydrophobic units.¹⁴ We also introduced hydrophobic polymers HE_n-DNA (Figure 2b) on one face of a DNA cube, and preliminarily showed their assembly into discrete aggregates, which we hypothesized to be cube dimer, tetramer, hexamer, etc.²⁴ With a very long alkyl component in HE_n-DNA (n=12) on one

1
2
3
4
5
6
7
8
9
10
11
12
13
14
15
16
17
18
19
20
21
22
23
24
25
26
27
28
29
30
31
32
33
34
35
36
37
38
39
40
41
42
43
44
45
46
47
48
49
50
51
52
53
54
55
56
57
58
59
60

face of a DNA cube, we showed the formation of a spherical micelle with a hydrophobic core, and DNA cubes on its exterior. This cube micelle displayed dynamic character (cubes can be removed by strand displacement), the ability to form higher-order micelle networks, and to act as a scaffold to organize fluorescent dyes into an antenna structure with controlled FRET.²⁴

To develop a better understanding of the rules for this hydrophobically driven assembly, it was crucial to further characterize the molecularity of the quantized cage aggregates. We thus examined the effect of the chain length of hydrophobic polymers HE_n-DNA on their assembly with DNA cages (Figure 3a, we name the DNA sequence on the polymer 'DNA'). Cube C₄ has four identical single-stranded stretches on one of its faces, each complementary to the DNA strand of the DNA-polymer conjugates. The decoration C₄ with four HE_n-DNA was achieved by mixing all components in magnesium-containing buffer then thermally annealing from 95°C to 4°C over 4 hours. The formation of DNA nanostructures was followed by native polyacrylamide gel electrophoresis (PAGE) as shown in Figure 3b. Addition of four complementary unmodified DNA strands to C₄ yielded a single band of lower electrophoretic mobility. Addition of strands with short hydrophobic chains to one face of cube C₄, from HE₁-DNA to HE₄-DNA, resulted in single bands of similar electrophoretic mobility compared to C₄ with unmodified DNA, consistent with a monomeric cube. The lack of difference in electrophoretic mobility for these cubes as the number of hydrophobic repeats in HE_n-DNA increases (n=1-4) is possibly consistent with some chain folding or interaction of these chains across one face of the cube in a manner that does not impede the movement of the assemblies on native PAGE. Thus, when DNA-polymer conjugates with 1-4 hydrophobic repeats were added to one face of the cube, monomeric structures decorated with hydrophobic groups are formed.

When longer hydrophobic chains from HE₅-DNA to HE₁₂-DNA were added to C₄, we no longer see the monomeric cube as a major product. Instead, we observe the combination of cubes into discrete aggregates. This is likely due to the increased hydrophobicity of the polymer chains attached to the cube, promoting cube association to hide these hydrophobic chains in the core (akin to a protein coiled-coil motif). The identity of C₄/HE₆-DNA was elucidated by atomic force microscopy (AFM). Figure 3c reveals elongated structures of two spheres, which accounted for 76% of population (cube dimers), and triangular structures with the edge length of ~30 nm (cube trimers, see below). Some disaggregation of the higher-order structures into individual cubes (diameter of ~17-18 nm) was also noted on the mica surface, and can be attributed to strong electrostatic interactions between DNA and mica, that compete with the hydrophobic interactions holding together the DNA nanostructures.²¹ The hydrodynamic size measured by dynamic light scattering (DLS) indicates that C₄/HE₆-DNA had low polydispersity, but was

1
2
3 not able to differentiate between the two populations of higher-order structures (Figure 3d, and see
4 Section XIX in Supporting Information for isolation of the individual higher-order structures).
5
6

7
8 To further support the identity of C₄/HE₆-DNA, we tagged each cube with a gold nanoparticle
9 (see Section VIII in Supporting Information) and preliminarily characterized the assemblies by
10 transmission electron microscopy (TEM). We observed a larger population of the clusters containing 2
11 and 3 AuNPs in close proximity (see Supplementary Figure 15). The technique was complicated by
12 sample-surface interactions, which sometimes resulted in populations of higher-order aggregates.
13
14 However, these observations are consistent with dimeric and trimeric structures as the identity of the
15 higher-order structures for C₄/HE₆-DNA.
16
17
18
19
20
21
22
23
24
25
26
27
28
29
30
31
32
33
34
35
36
37
38
39
40
41
42
43
44
45
46
47
48
49
50
51
52
53
54
55
56
57
58
59
60

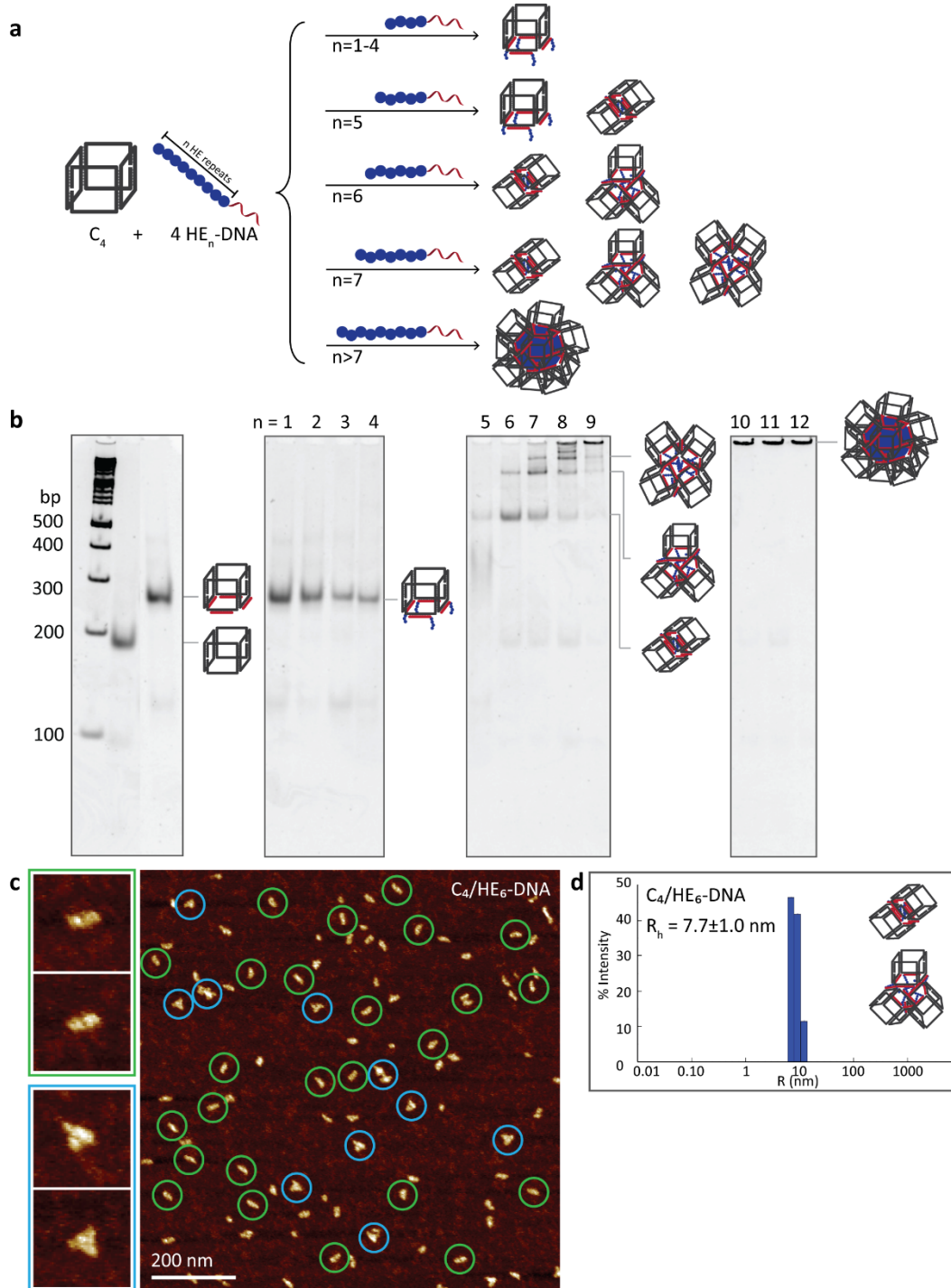


Figure 3. Decoration of one face of C_4 with four HE_n -DNA ($n=1-12$). a) Assembly products of C_4 with HE_n -DNA. Finite cube aggregation number that scales with the number of hydrophobic polymer repeats are observed. b) Native PAGE showing the assembly of C_4 , C_4 /DNA and C_4/HE_n -DNA. c) AFM image of C_4/HE_6 -DNA showing cube dimers (green circles) and cube trimers (blue circles). d) Size distribution

1
2
3 histogram of C₄/HE₆-DNA obtained from DLS. (see Supplementary Figure 26 for additional AFM
4 images)
5
6

7
8 As the number of hydrophobic HE repeats on the polymer increased, increasingly large
9 superstructures were formed. Interestingly, their aggregation number correlated with the number of HE
10 repeats. Comparison of these bands to the DNA ladder allowed an estimation of relative ‘molecular
11 weight’ for each higher-order structure, and we can calculate a cube aggregation number by comparing
12 these molecular weights to that of the monomeric structure. The results suggest that the cube aggregation
13 number gradually increases by increments of one (see Section VII in Supporting Information). Thus, HE₇-
14 DNA gives dimer, trimer and tetramer, and HE₈-DNA gives trimer, tetramer and pentamer. HE₉-DNA to
15 HE₁₂-DNA give non-penetrating bands, which may be composed of incrementally higher cube
16 aggregation numbers. However, it should be noted that the relationship between cube aggregation number
17 and electrophoretic mobility can also be nonlinear.
18
19
20
21
22
23

24 ***Polymers: sequences of the polymers and relative numbers of hydrophilic to hydrophobic repeats***

25
26
27 The monomer sequence along polymer chains can significantly influence polymer physical
28 properties. To investigate this effect on DNA cages, we assembled cube C₄ with a series of copolymers of
29 different sequences, all containing a constant number of 6 hydrophobic HE and 6 hydrophilic HEG
30 repeats per chain. This includes alternating chains of single monomers (HE-HEG)₆-DNA, two monomers
31 (HE₂-HEG₂)₃-DNA, three monomers (HE₃-HEG₃)₂-DNA and six monomers (Figure 4a). The latter
32 polymer has two sequences; HEG₆-HE₆-DNA, in which the hydrophobic portion is between the DNA and
33 HEG chains, and HE₆-HEG₆-DNA, in which the hydrophobic portion is at the chain-end. Only the latter
34 structure among this copolymer series was previously shown to assemble into micellar aggregates,
35 whereas the other structures remain as unimers in solution.¹⁵
36
37
38
39
40
41

42
43 Decoration of these HE/HEG-DNA polymers on cube C₄ yielded monomeric structures (Figure
44 4b, with one exception, see below). The electrophoretic mobility of these structures on native PAGE
45 increased with HE block length, consistent with greater structure compaction. As the HE block becomes
46 longer, the local hydrophobicity of individual HE segments increases, thus potentially enabling more
47 efficient folding of the hydrophobic chains, which can make the structures increasingly compact and
48 increases their gel mobility. Interestingly, these polymers did not result in cube aggregation, despite their
49 relatively high hydrophobic content. These cages are especially interesting for applications in cellular
50 delivery: they behave as monomers, yet their hydrophobic content can facilitate interaction with cellular
51 membranes and modify their delivery profile.^{18,19,25,26} It is of note that this behavior is a direct result of
52
53
54
55
56
57
58
59
60

1
2
3
4
5
6
7
8
9
10
11
12
13
14
15
16
17
18
19
20
21
22
23
24
25
26
27
28
29
30
31
32
33
34
35
36
37
38
39
40
41
42
43
44
45
46
47
48
49
50
51
52
53
54
55
56
57
58
59
60

sequence control of the polymers, where regular block copolymers would not be able to generate this property.

The exception to this monomeric assembly was C₄/HE₆-HEG₆-DNA, which gave higher-order structures that appeared as a non-penetrating band on the native PAGE. The AFM images (Figure 4c) reveal polygonal rings containing 3-5 vertices with edge length of ~30 nm. The size of the structures was also supported by DLS measurements (R_h=14 nm). We believe that the flexible HEG block is able to serve as a spacer between hydrophobic HE domains and the cubes. The HE block of HE₆-HEG₆-DNA can form hydrophobic domains by interacting with the chains on the other cubes side-to-side, resulting in polygonal rings. As the HEG block might be a crucial parameter for the diameter of the ring-like structures, we hypothesized that a longer HEG block could create structures with larger spacing between the cubes. The hydrodynamic radius of C₄/HE₆-HEG₁₂-DNA (18 nm) was indeed significantly larger than that of C₄/HE₆-HEG₆-DNA. However, in this case, we also observed disassembly of some of the structures on the mica surface by AFM, which is likely due to the larger hydrophilic-to-hydrophobic content of this polymer (Figure 4c).

To further increase the stability of this hydrophobic inter-scaffold 'handshake', we assembled C₄/HE₁₂-HEG₆-DNA, which has a longer hydrophobic HE block than C₄/HE₆-HEG₆-DNA. This molecule generated a high yield of well-defined ring-like structures with hollow features in the middle as observed by AFM (Figure 4c). Further increasing the length of the HEG block to C₄/HE₁₂-HEG₁₂-DNA also showed efficient formation of ring structures, which looked denser by AFM. The radii of both structures were comparable (20 nm/27 nm (DLS/AFM) for C₄/HE₁₂-HEG₆-DNA; 21/24 nm (DLS/AFM) for C₄/HE₁₂-HEG₁₂-DNA, Figure 4c and see Section XI in Supporting Information for DLS). TEM characterization also confirmed the presence of relatively homogeneous spherical structures (radius 12 nm for C₄/HE₁₂-HEG₆-DNA and 15 nm for C₄/HE₁₂-HEG₁₂-DNA, see Section XIII in Supporting Information). It should be noted that the sizes obtained from AFM and DLS were similar to one another, and were significantly larger than those obtained by TEM, suggesting that the structures may be ring-like in solution. The possible explanation for the smaller sizes measured by TEM is a collapse of the structures on the hydrophobic carbon-coated grids and the drying of DNA structures under high vacuum.²⁷

The estimated yields of the doughnut-shaped structures obtained by examination of the AFM images were high in all cases, except for the sequence in which the HE block is short (6 units) as compared to the HEG block (12 units). It was difficult to provide a precise yield from the AFM images, because of the presence of some misassembled structures of unknown composition in the image

1
2
3 **background.** Thus, we can conclude that the addition of HEG repeats provides a spacer between DNA
4 scaffolds and yields ring structures. To our knowledge, the assembly of DNA cages into ‘doughnut-like’
5 ring structures is unprecedented. It is interesting that, despite the flexibility of both HE and HEG chains,
6 we observed discrete cube assemblies here, rather than linear oligomers.
7
8
9
10
11
12
13
14
15
16
17
18
19
20
21
22
23
24
25
26
27
28
29
30
31
32
33
34
35
36
37
38
39
40
41
42
43
44
45
46
47
48
49
50
51
52
53
54
55
56
57
58
59
60

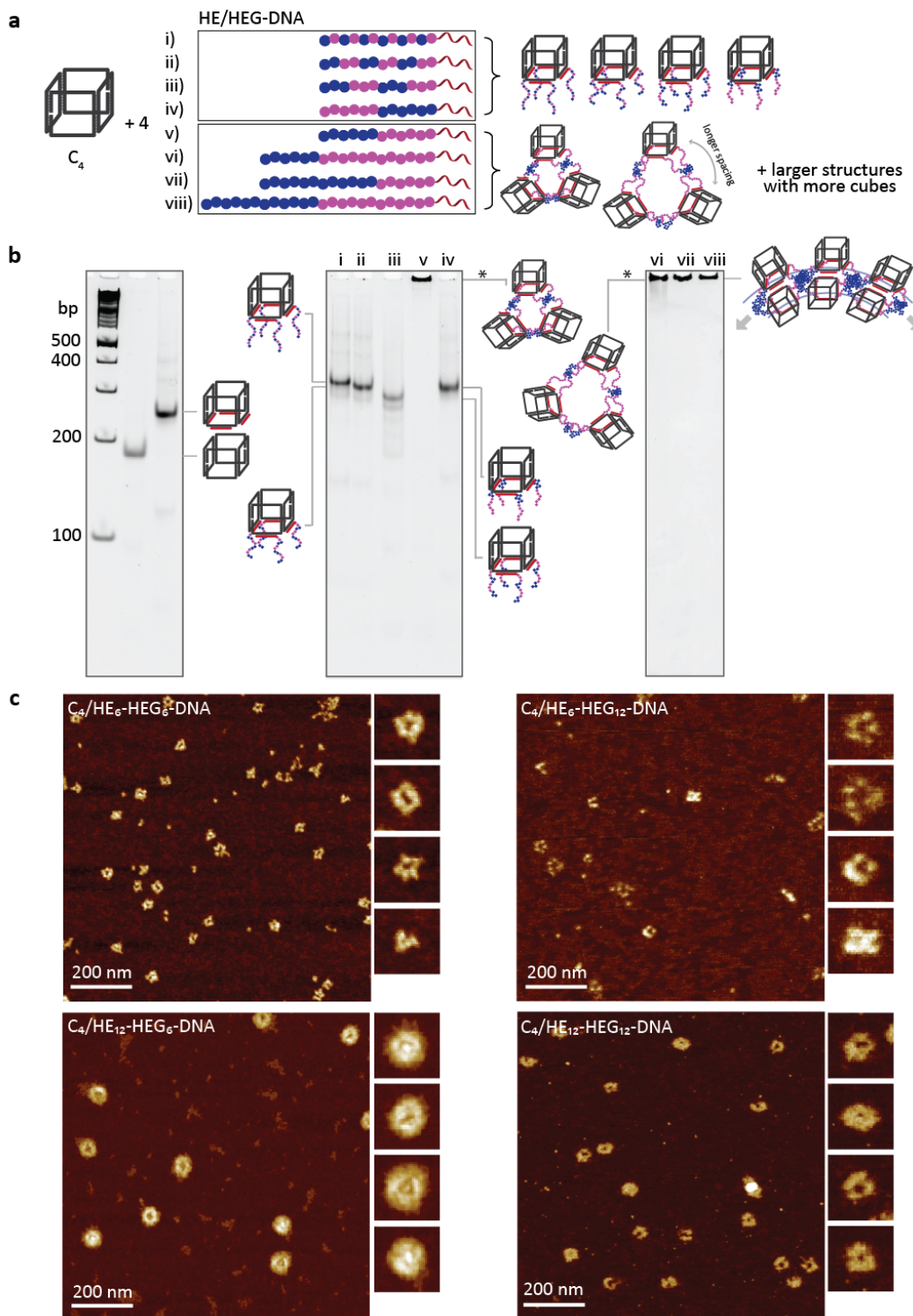


Figure 4. Decoration of C_4 with four HE/HEG-DNA. a) Assembly products of C_4 with HE/HEG-DNA. The polymer sequences can dictate whether the assembly either yields a monomeric cube or forms higher-order structure. b) Native PAGE showing the assembly of C_4 , C_4/DNA , C_4 with HE/HEG-DNA. *Only

1
2
3 the schematics of 3-vertices rings were shown here for C_4/HE_6-HEG_6-DNA and $C_4/HE_6-HEG_{12}-DNA$. c)
4 AFM images of C_4 with HE_n-HEG_m-DNA ($n=6,12$ and $m=6,12$). The presence of HEG block in the
5 polymer chains can increase the spacing between the cubes.
6
7

9 *Cages: orientation of the polymer chains on the cages*

10
11 We previously reported that 8 dendritic HE units attached on both faces of a DNA cube result in
12 an intramolecular association, with the ability to encapsulate molecules in the internal hydrophobic
13 environment.¹⁴ We were interested in probing the dependence of this phenomenon on polymer
14 architecture and chain length (e.g., how many how many hydrophobic chains can fit inside the cage?).
15
16 Cube C_8 was designed to allow decoration with up to 8 polymer chains on both its top and bottom faces
17 (Figure 5a). A one-pot assembly of C_8 with HE_n-DNA was performed. In Figure 5b, short HE chains
18 generated monomeric structures with a sharp band on the gel. Interestingly, as the number of hydrophobic
19 repeats increased, the electrophoretic mobility of this band increased (rather than decreased); it then
20 remained constant at HE_4-DNA until HE_6-DNA . The structure of C_8/HE_6-DNA was characterized by
21 AFM, which revealed mostly single spherical features with a radius of 9.6 ± 4.8 nm, comparable to C_8 (see
22 Supplementary Figures 32 and 33). DLS measurements (Figure 5c) indicated that C_8/HE_6-DNA
23 ($R_h=6.4\pm 0.3$ nm) was smaller than C_8/DNA ($R_h=7.1\pm 0.6$ nm). A likely assembly mode here is that HE
24 chains (HE_4-HE_6) collapse and create a hydrophobic core inside the cube, resulting in a more compact
25 structure similar to that of dendritic HE chains.¹⁴ The formation of the hydrophobic core in C_8/HE_6-DNA
26 was further supported by the encapsulation of hydrophobic Nile Red fluorescent dye.²⁸ Compared to a
27 cube decorated with unmodified DNA, there was a significantly higher fluorescent signal of Nile Red in
28 C_8/HE_6-DNA (Figure 5d).
29
30
31
32
33
34
35
36
37
38
39

40 As the number of hydrophobic repeats on the polymer increased, HE_7-DNA started to form a
41 cube dimer and longer hydrophobic chains resulted in higher-order structures as the major product. Thus,
42 up to 6 HE chains per polymer can be accommodated in the cube core (a total of 48 HE chains), beyond
43 which intermolecular assembly sets in. Both AFM and DLS measurements suggested that extended
44 structures formed in the case of C_8/HE_8-DNA and $C_8/HE_{12}-DNA$ (see Section XI and XII in Supporting
45 Information for DLS and AFM).
46
47
48
49
50
51
52
53
54
55
56
57
58
59
60

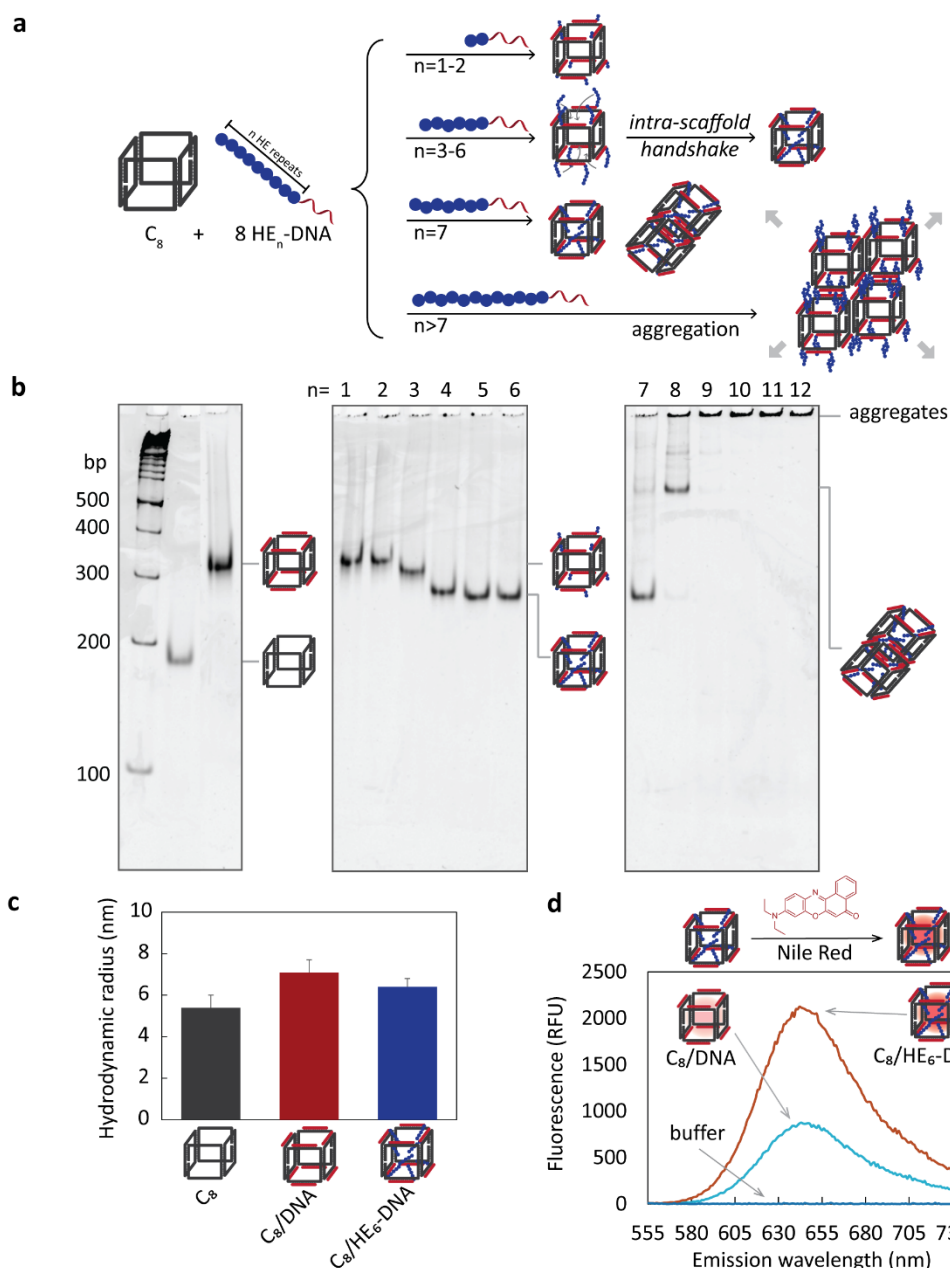


Figure 5. C_8 assembly with $\text{HE}_n\text{-DNA}$ ($n=1,12$) on its two faces. a) Assembly products of C_8 with $\text{HE}_n\text{-DNA}$. Medium chain length of hydrophobic polymers ($n=3-6$) prefers ‘intra-scaffold handshake’ and create hydrophobic core inside the cube. b) Native PAGE showing the assembly products of C_8 , C_8/DNA and $C_8/\text{HE}_n\text{-DNA}$. c) Hydrodynamic radii of C_8 , C_8/AT (7.1 ± 0.6 nm) and $C_8/\text{HE}_6\text{-AT}$ (6.4 ± 0.4 nm). d) Fluorescent traces of Nile Red molecules encapsulated inside C_8/DNA and $C_8/\text{HE}_6\text{-DNA}$. The signal of Nile Red was higher in the presence of $\text{HE}_6\text{-AT}$. No fluorescent signal was observed in the buffer (see Supporting Information section XIV for details). These observations suggest the formation of hydrophobic core inside the cube.

Cages: structures and sizes of the cages

The clip-by-clip approach allows the efficient construction of cages with various geometries and sizes. This geometric variation offers more design parameters to control the number and the orientation of the polymers on the cages. It allows us to answer the question: can the cage geometry change the onset of assembly? To investigate this effect, triangular prism (TP) and pentagonal prism (PP) were assembled with HE_n-DNA in an analogous way to the cube C/HE_n-DNA. With these chains on one face of the cage, the hydrophobically driven aggregation numbers for TP₃ and PP₅ were indeed different from those of the cube C₄. With HE₆-DNA on one face, TP₃ gave dimer, trimer and tetramer while C₄ and PP₅ gave only dimer and trimer (see Supplementary Figure 6 and 7 for TP₃ and PP₅). This can be explained by the smaller size of the triangular prism, allowing more cages to fit around the hydrophobic core. Thus, aggregation number can be tuned with the cage geometry.

With HE_n-DNA on both faces, we expect that the smaller triangular prism can accommodate shorter polymer chains in its core than the cube, and the pentagonal prism would encapsulate larger polymer chains. Indeed, TP₆ could accommodate lengths up to HE₅ within its core (capacity 30 HE units), before the cage started to dimerize with HE₆; this transition occurred from HE₆ to HE₇ for the cube (capacity 48 HE units), and from HE₇ to HE₈ for the pentagonal prism (capacity 70 HE units, Figure 6a). The larger cages and higher total number of HE repeats per cage can in principle increase the loading capacity of hydrophobic guests. To verify this, we compared the loading capacity of the three different cages decorated with HE₆-DNA (Figure 6b). The results showed an approximately 2.5-fold increase in Nile Red loading capacity when the size of cages and thus total number of HE₆-DNA increased: 9.1±1.7 molecules per PP₁₀/HE₆-DNA, 3.6±1.2 molecules per C₈/HE₆-DNA and 1.5±0.4 molecules per TP₆/HE₆-DNA.

We had previously shown that the HE₆-DNA conjugate forms micelles with a diameter of ~13 nm.¹⁵ Yet if this polymer is fully stretched, it has a ~7 nm long DNA portion and a ~12 nm long hydrophobic chain. Considering the efficient chain packing of polyethylene²⁹ and the fact that HE chains are punctuated by phosphate groups, it is possible that they fold upon themselves to enable tight packing between adjacent HE repeats¹⁵ in a similar way to the arrangement of phospholipid bilayers and bola-amphiphiles.^{30,31} This would result in a smaller micelle size and a tighter, more densely packed hydrophobic core. The same tight chain packing may be present in the core of the ‘micellar cages’ above, which may explain their relatively low loading capacity. It has been shown that the crystallinity of the hydrophobic core of block copolymer micelles tends to decrease the loading capacity for guest molecules, because of lower chain mobility that hinders the diffusion of the hydrophobic molecules.³²⁻³⁴ While

additional studies need to be performed to better understand the chain packing in our ‘micellar cages’, we will also examine reducing the extent of core packing by using unsaturated lipids, rather than HE chains as the hydrophobic units.

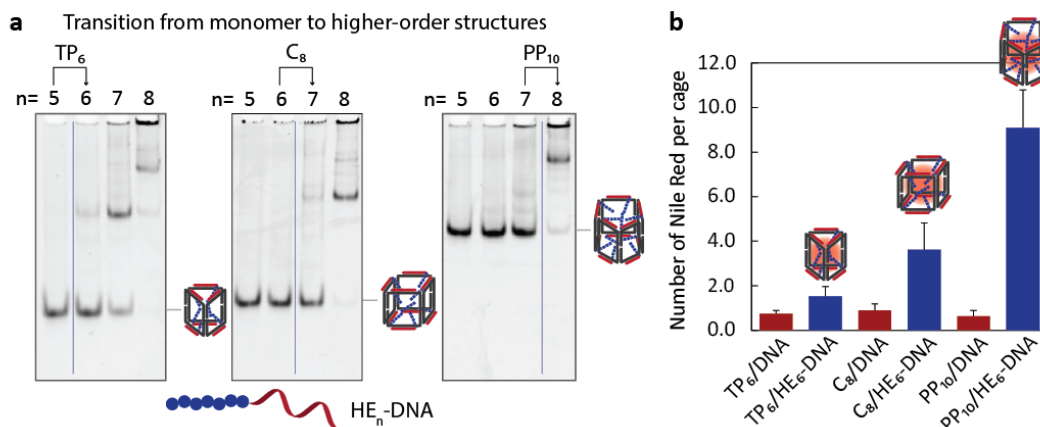


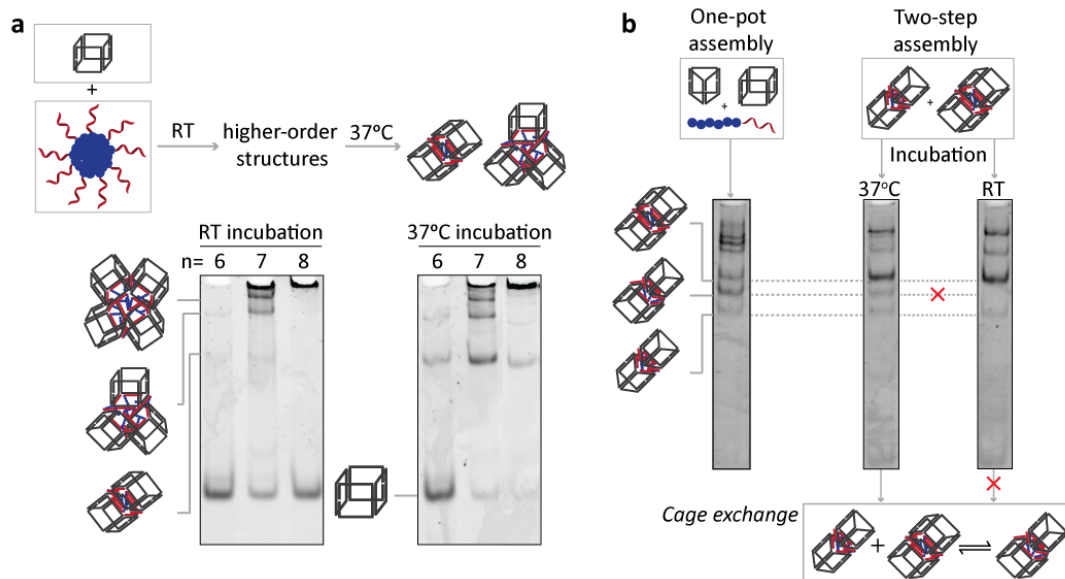
Figure 6. Effect of the cage's structure. a) Native PAGE showing the assembly products of triangular prism TP₆, cube C₈ and pentagonal prism PP₁₀ with HE₅-DNA to HE₉-DNA. Larger cages could provide more space for the hydrophobic core and therefore can accommodate longer HE_n-DNA without forming higher-order structures. (HE₅-DNA for TP₆, HE₆-DNA for C₈ and HE₇-DNA for PP₁₀). b) Nile Red encapsulation in double-stranded cages (red bars) and cages decorated with HE₆-DNA (blue bars). There was a ~2.5-fold increase in loading capacity with increased cage size.

Assembly dynamics and thermodynamic properties

The cage architectures described here were all generated by a one-step thermal annealing protocol (95 to 4°C) where all component strands and DNA polymers are mixed and annealed together. There are two possible mechanisms for their assembly: (i) as the strands are cooled from 95°C, the cage assembles first, followed by hybridization to the individual DNA-polymer strands; then subsequent hydrophobic interactions drive the assembly of super-structures as the temperature further decreases. (ii) the DNA cage and the micelles pre-form separately, and the two objects hybridize together into the final structure, thus transitioning from a micelle morphology to cube superstructures. To explore this mechanistic aspect, we pre-assembled cube C₄ and HE_n-DNA separately, and then incubated them together at room temperature for 30 minutes (see Supplementary Figure 58). Short HE chains (HE₁-DNA to HE₄-DNA) that are not expected to form stable micelles yielded monomeric structures similar to the one-pot assembly. On the other hand, the two-step assembly process with longer chains (HE₆-DNA to HE₁₂-DNA) resulted in non-

penetrating bands, as well as unfunctionalized DNA cube. (Figure 7a and see Supplementary Figure 58 in Supporting Information). Thus, in this case, the cube cannot disassemble pre-formed micelles in order to hybridize with their individual chains at room temperature. Interestingly for HE₇-DNA and HE₈-DNA, increasing the incubation temperature to 37°C converted the mixture of higher-order structures and cube into the cube dimers and trimers observed earlier (Figure 7a and see Supplementary Figure 59 and Supplementary Figure 60 for temperature dependence). At this temperature, the HE chains in the micelle may possibly rearrange into the more thermodynamically favorable cube-aggregate state. Thus a pre-formed DNA-polymer spherical micelle can shape-shift into quantized cage assemblies, merely by adding DNA cages at 37°C.

The second question that we would like to address is the possibility of shape discrimination, i.e., whether two DNA cages of the same geometry would prefer to associate together via hydrophobic interactions. In a one-pot annealing of HE₆-DNA with both the triangular prism TP₃ and cube C₄ strands, we found no selectivity in the cage structures: for example, homo- and heterodimer combinations of TP₃-TP₃, TP₃-C₄ and C₄-C₄ were observed (Figure 7b, left gel). However, if TP₃-TP₃ and C₄-C₄ homodimers were separately generated and mixed together at room temperature for 30 minutes, no observable exchange occurred. (Figure 7b, right gel). At 37°C, scrambling started to happen (Figure 7b, middle gel). Additionally, we verified the formation of this heterodimer by labeling each of the cube C₄ and triangular prism TP₃ with two dyes of different emission colors, and observing co-localization by gel electrophoresis imaging (Supplementary Figure 64). Because of its stability at room temperature, it is possible to isolate the heterodimer (for example, TP₃-C₄) to generate anisotropic nanoparticles, whose free single-stranded faces can be of different sequences and can provide unique sites for further functionalization.



1
2
3 **Figure 7.** Assembly dynamics of the quantized structures. a) Mixing of separately pre-assembled cubes
4 and HE_n-DNA (n=6,8) micelles generated larger aggregates. Increasing incubation temperature converted
5 these structures back to small structures (dimers, trimers and tetramers) observed in the one-pot assembly.
6
7 b) As representative examples, only the bands corresponding to dimers were labeled. One-pot annealing
8 of TP₃, C₄ and HE₆-DNA generated all cage combinations such as dimers of TP₃/TP₃, TP₃/C₄ and C₄/C₄
9 (left gel). Mixing separately preformed TP₃/HE₆-DNA and C₄/HE₆-DNA at room temperature did not
10 result in exchange (right gel). Incubation at 37°C for 30 minutes resulted in scrambling to the heterodimer
11 (TP₃/C₄).
12
13
14
15
16
17
18
19

20
21
22
23
24
25
26
27
28
29
30
31
32
33
34
35
36
37
38
39
40
41
42
43
44
45
46
47
48
49
50
51
52
53
54
55
56
57
58
59
60

Decoration of HE₆-DNA on the cube C₈ with 8 binding sites resulted in a totally different mode of HE chain interactions, as compared to cube C₄. Here, the pre-organization of 8 HE₆ chains on C₈ increased the extent of intra-scaffold ‘handshake’ of these chains over inter-scaffold ‘handshake’. This is likely due to the lower entropic penalty of the intramolecular assembly, and the increase in the effective concentration of HE₆ in the DNA cage core, thus favoring micellization below the critical micelle concentration of the polymers.¹⁵ Thermal denaturation analysis was performed to investigate the thermodynamic properties of these ‘micellar cage’. Interestingly, the presence of HE₆ chains in the core of the cube provided significant stabilization of C₈/DNA, with an increase of 5.5°C in thermal denaturation (Figure 8a). The full width at half-maximum (FWHM) determined from the first derivatives of the melting curves can be used as the indication for the degree of cooperativity.^{35,36} The dramatic decrease in FWHM of C₈/HE₆-DNA (4.0±0.1°C) in comparison to C₄/DNA (10.1±1.0°C) indicated a significantly increased positive cooperativity of DNA nanostructure assembly/disassembly. To confirm this cooperativity, we performed a titration experiment, in which increasing quantities of HE₆-DNA were added to C₈ (Supplementary Figure 56). All-or-none binding was observed with sub-stoichiometric amounts of the DNA polymer with respect to the cube binding sites. On the other hand, titration of C₈ with unmodified DNA strands gave intermediate structures and did not exhibit such a cooperativity (Supplementary Figure 56). Thus with the intra-scaffold handshake, the DNA base-pairing and hydrophobic effects are acting synergistically, providing greater stability and assembly cooperativity to the cube-micelle structures. This is of significant importance for the biological applications of these structures.

We hypothesized that decoration of HE₆-DNA on only one face of the cage (C₄) would not affect DNA hybridization to the same extent. C₄/HE₆-DNA exhibited a slight increase of 2°C in T_m compared to C₄/DNA (Figure 8b). Interestingly, increased cooperativity was also observed in this system, as indicated

by a significant decrease in FWHM ($10.3\pm 1.8^\circ\text{C}$ for C_4/DNA and $4.5\pm 0.7^\circ\text{C}$ for $C_4/\text{HE}_6\text{-DNA}$). A comparable increase in T_m and decrease in FWHM was observed for $C_4/\text{HE}_{12}\text{-DNA}$. Moreover, some extra stabilization was also observed in assemblies with block copolymers $\text{HEG}_n\text{-HE}_n\text{-DNA}$. Hence, the hydrophobic HE chains contribute to greater stabilization and cooperativity for DNA assemblies; this additional stabilization possibly stems from some additional intra-scaffold interactions between HE chains, providing extra cohesion to the assembly. Therefore, the hydrophobic interactions can not only introduce new DNA assembly modes but also synergistically work together with the base-pairing interactions to form and stabilize the DNA nanostructures.

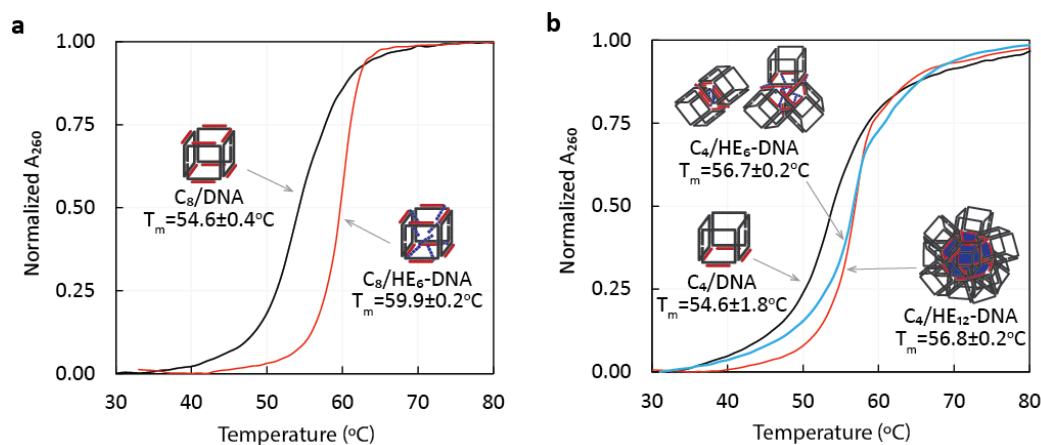


Figure 8. Melting profiles of the assemblies of a) C_8/DNA and $C_8/\text{HE}_6\text{-DNA}$; b) C_4/DNA , $C_4/\text{HE}_6\text{-DNA}$ and $C_4/\text{HE}_{12}\text{-DNA}$. An increase in melting temperature (T_m) of the cubes with $\text{HE}_n\text{-DNA}$ suggested the synergistic stabilization of DNA nanostructures by the hydrophobic interactions. The narrow transition of the curve is consistent with a large increase in cooperativity of DNA hybridization/dissociation in the presence of hydrophobic chains.

Conclusion

We have demonstrated the use of sequence-defined hydrophobic polymers to provide orthogonal assembly modes to DNA cages and to synergistically work together with base pairing interactions. A range of new structures can be accessed by fine-tuning of the length of hydrophobic blocks, the sequence order of the polymers and the orientation of the polymers on the cages. Short hydrophobic chains result in monomeric DNA cage structures that are decorated with alkyl or oligoethylene glycol units. Longer hydrophobic chains arranged on one face of the DNA prismatic cage result in quantized cube higher-order structures; here, the number of hydrophobic repeats defines the number of DNA cages that form these

1
2
3 aggregates. When these hydrophobic chains are organized on both faces of the cage, these chains point to
4 the interior of the cage and undergo an intra-scaffold 'handshake'. The sequence order of hydrophobic
5 and hydrophilic monomers on the polymer chains can significantly control the interactions between
6 hydrophobic blocks, resulting in monomeric cages and 'doughnut-shaped' DNA cage-ring structures for
7 specific sequences. These DNA-polymer nanostructures can be alternatively viewed as amphiphilic block
8 copolymers, where the hydrophilic block consists of a DNA cage, and the hydrophobic block has
9 hexaethylene chains. However, unlike block copolymers, the two components are monodisperse,
10 sequence defined, and the placement of hydrophobic polymers on the DNA cage is anisotropic. This gives
11 rise to entirely new morphologies that are not observed with block copolymers, and provides guidelines
12 for the design of DNA nanostructures mediated by hydrophobic interactions. It is remarkable that high
13 specificity is achieved in these assembled structures despite the fact that the hydrophobic effect is one of
14 the least directional supramolecular interactions. We have only worked with hydrophobic interactions so
15 far, but the potential for structural complexity and protein-inspired folding is tremendous when additional
16 interactions (fluorophilic, metal-binding, etc.) are introduced.
17
18
19
20
21
22
23
24
25
26
27
28

29 **Supporting Information.** DNA cage design and assembly, determination of cage aggregation number,
30 gold nanoparticle labeling, characterization by DLS, AFM and TEM, Nile red encapsulation, studies of
31 stability and cooperativity, effect of cage geometry and concentration, isolation of cage aggregates.
32
33
34

35 **AUTHOR INFORMATION**

36 **Corresponding Author**

37
38
39
40 *hanadi.sleiman@mcgill.ca
41
42

43 **Acknowledgements**

44
45 The authors thank NSERC, CFI, CSACS, CIHR and FQRNT for funding. H.F.S. is a Cottrell Scholar of
46 the Research Corporation. We thank Dr. Alexander Wahba for his help with MS characterization.
47
48

49 **References**

- 50
51
52 (1) Lutz, J.-F.; Ouchi, M.; Liu, D. R.; Sawamoto, M. *Science* **2013**, *341*.
53 (2) Aldaye, F. A.; Palmer, A. L.; Sleiman, H. F. *Science* **2008**, *321*, 1795.
54 (3) Winfree, E.; Liu, F.; Wenzler, L. A.; Seeman, N. C. *Nature* **1998**, *394*, 539.
55 (4) Yan, H.; Park, S. H.; Finkelstein, G.; Reif, J. H.; LaBean, T. H. *Science* **2003**, *301*, 1882.
56 (5) Liu, D.; Wang, M.; Deng, Z.; Walulu, R.; Mao, C. *J. Am. Chem. Soc.* **2004**, *126*, 2324.
57 (6) He, Y.; Chen, Y.; Liu, H.; Ribbe, A. E.; Mao, C. *J. Am. Chem. Soc.* **2005**, *127*, 12202.
58
59
60

- 1
2
3
4 (7) Chen, J. H.; Seeman, N. C. *Nature* **1991**, *350*, 631.
5 (8) Rothmund, P. W. *Nature* **2006**, *440*, 297.
6 (9) Aldaye, F. A.; Sleiman, H. F. *J. Am. Chem. Soc.* **2007**, *129*, 13376.
7 (10) McLaughlin, C. K.; Hamblin, G. D.; Aldaye, F. A.; Yang, H.; Sleiman, H. F. *Chem. Commun.*
8 **2011**, *47*, 8925.
9 (11) Wei, B.; Dai, M.; Yin, P. *Nature* **2012**, *485*, 623.
10 (12) Mai, Y.; Eisenberg, A. *Chem. Soc. Rev.* **2012**, *41*, 5969.
11 (13) Woo, S.; Rothmund, P. W. K. *Nat Chem* **2011**, *3*, 620.
12 (14) Edwardson, T. G.; Carneiro, K. M.; McLaughlin, C. K.; Serpell, C. J.; Sleiman, H. F. *Nat*
13 *Chem* **2013**, *5*, 868.
14 (15) Edwardson, T. G.; Carneiro, K. M.; Serpell, C. J.; Sleiman, H. F. *Angew. Chem. Int. Ed.*
15 **2014**, *53*, 4567.
16 (16) Chen, Y.-J.; Groves, B.; Muscat, R. A.; Seelig, G. *Nat Nano* **2015**, *10*, 748.
17 (17) Bujold, K. E.; Fakhoury, J.; Edwardson, T. G. W.; Carneiro, K. M. M.; Briard, J. N.; Godin,
18 A. G.; Amrein, L.; Hamblin, G. D.; Panasci, L. C.; Wiseman, P. W.; Sleiman, H. F. *Chem. Sci.* **2014**, *5*, 2449.
19 (18) Hamblin, G. D.; Carneiro, K. M.; Fakhoury, J. F.; Bujold, K. E.; Sleiman, H. F. *J Am Chem*
20 *Soc* **2012**, *134*, 2888.
21 (19) Fakhoury, J. J.; McLaughlin, C. K.; Edwardson, T. W.; Conway, J. W.; Sleiman, H. F.
22 *Biomacromolecules* **2014**, *15*, 276.
23 (20) Lee, H.; Lytton-Jean, A. K. R.; Chen, Y.; Love, K. T.; Park, A. I.; Karagiannis, E. D.; Sehgal,
24 A.; Querbes, W.; Zurenko, C. S.; Jayaraman, M.; Peng, C. G.; Charisse, K.; Borodovsky, A.; Manoharan, M.;
25 Donahoe, J. S.; Truelove, J.; Nahrendorf, M.; Langer, R.; Anderson, D. G. *Nat Nano* **2012**, *7*, 389.
26 (21) List, J.; Weber, M.; Simmel, F. C. *Angew. Chem. Int. Ed.* **2014**, *53*, 4236.
27 (22) Zhou, C.; Wang, D.; Dong, Y.; Xin, L.; Sun, Y.; Yang, Z.; Liu, D. *Small* **2015**, *11*, 1161.
28 (23) Wilks, T. R.; Bath, J.; de Vries, J. W.; Raymond, J. E.; Herrmann, A.; Turberfield, A. J.;
29 O'Reilly, R. K. *ACS Nano* **2013**, *7*, 8561.
30 (24) Serpell, C. J.; Edwardson, T. G.; Chidchob, P.; Carneiro, K. M.; Sleiman, H. F. *J. Am. Chem.*
31 *Soc.* **2014**, *136*, 15767.
32 (25) Ko, S.; Liu, H.; Chen, Y.; Mao, C. *Biomacromolecules* **2008**, *9*, 3039.
33 (26) Walsh, A. S.; Yin, H.; Erben, C. M.; Wood, M. J. A.; Turberfield, A. J. *ACS Nano* **2011**, *5*,
34 5427.
35 (27) Buckhout-White, S.; Ancona, M.; Oh, E.; Deschamps, J. R.; Stewart, M. H.; Blanco-
36 Canosa, J. B.; Dawson, P. E.; Goldman, E. R.; Medintz, I. L. *ACS Nano* **2012**, *6*, 1026.
37 (28) Greenspan, P.; Mayer, E. P.; Fowler, S. D. *J. Cell Biol.* **1985**, *100*, 965.
38 (29) Ehrenstein, G. W.; Theriault, R. P. *Polymeric materials : structure, properties,*
39 *applications*; Hanser ; Hanser Gardner Publications: Munich; Cincinnati, OH, 2001.
40 (30) Fuhrhop, J.-H.; Wang, T. *Chem. Rev.* **2004**, *104*, 2901.
41 (31) Blume, A.; Drescher, S.; Meister, A.; Graf, G.; Dobner, B. *Faraday Discuss.* **2013**, *161*,
42 193.
43 (32) Shuai, X.; Ai, H.; Nasongkla, N.; Kim, S.; Gao, J. *J. Controlled Release* **2004**, *98*, 415.
44 (33) Glavas, L.; Odelius, K.; Albertsson, A.-C. *Polym. Adv. Technol.* **2015**, *26*, 880.
45 (34) Gou, J.; Feng, S.; Xu, H.; Fang, G.; Chao, Y.; Zhang, Y.; Xu, H.; Tang, X. *Biomacromolecules*
46 **2015**, *16*, 2920.
47 (35) Eryazici, I.; Prytkova, T. R.; Schatz, G. C.; Nguyen, S. T. *J. Am. Chem. Soc.* **2010**, *132*,
48 17068.
49 (36) Greschner, A. A.; Toader, V.; Sleiman, H. F. *J. Am. Chem. Soc.* **2012**, *134*, 14382.
50
51
52
53
54
55
56
57
58
59
60

